Received: 8 May 2019 | Revised: 19 June 2019 | Accepted: 19 June 2019

DOI: 10.1111/jace.16655

ORIGINAL ARTICLE

Journal of the American Ceramic Society

Assessment of interatomic parameters for the reproduction of borosilicate glass structures via DFT-GIPAW calculations

Mariagrazia Fortino[1] | **Alessandro Berselli**[1] | **Nicholas Stone-Weiss**[2] | **Lu Deng**[3] | **Ashutosh Goel**[2] | **Jincheng Du**[3] | **Alfonso Pedone**[1]

[1]Department of Chemical and Geological Sciences, University of Modena and Reggio Emilia, Modena, Italia

[2]Department of Materials Science and Engineering, The State University of New Jersey, Rutgers, Piscataway, New Jersey

[3]Department of Materials Science and Engineering, University of North Texas, Denton, Texas

Correspondence
Alfonso Pedone, Department of Chemical and Geological Sciences, University of Modena and Reggio Emilia, Modena, Italia.
Email: alfonso.pedone@unimore.it

Funding information
U.S. National Science Foundation, Grant/Award Number: 1507131 and 1508001

Abstract

Borates and borosilicates are potential candidates for the design and development of glass formulations with important industrial and technological applications. A major challenge that retards the pace of development of borate/borosilicate based glasses using predictive modeling is the lack of reliable computational models to predict the structure-property relationships in these glasses over a wide compositional space. A major hindrance in this pursuit has been the complexity of boron-oxygen bonding due to which it has been difficult to develop adequate B–O interatomic potentials. In this article, we have evaluated the performance of three B–O interatomic potential models recently developed by Bauchy et al [*J. Non-Cryst. Solids*, 2018, 498, 294–304], Du et al [*J. Am. Ceram. Soc.* https://doi.org/10.1111/jace.16082] and Edèn et al [*Phys. Chem. Chem. Phys.*, 2018, 20, 8192–8209] aiming to reproduce the short-to-medium range structures of sodium borosilicate glasses in the system 25 Na_2O x B_2O_3 (75 − x) SiO_2 (x = 0-75 mol%). To evaluate the different force fields, we have computed at the density functional theory level the NMR parameters of ^{11}B, ^{23}Na, and ^{29}Si of the models generated with the three potentials and the simulated MAS NMR spectra compared with the experimental counterparts. It was observed that the rigid ionic models proposed by Bauchy and Du can both reliably reproduce the partitioning between BO_3 and BO_4 species of the investigated glasses, along with the local environment around sodium in the glass structure. However, they do not accurately reproduce the second coordination sphere of silicon ions and the Si–O–T (T = Si, B) and B-O-T distribution angles in the investigated compositional space which strongly affect the NMR parameters and final spectral shape. On the other hand, the core-shell parameterization model proposed by Edén underestimates the fraction of BO_4 species of the glass with composition $25Na_2O$ $18.4B_2O_3$ $56.6SiO_2$ but can accurately reproduce the shape of the ^{11}B and ^{29}Si MAS-NMR spectra of the glasses investigations due to the narrower B–O–T and Si-O-T bond angle distributions. Finally, the effect of the number of boron atoms (also distinguishing the BO_3 and BO_4 units) in the second coordination sphere of the network former cations on the NMR parameters have been evaluated.

KEYWORDS
borosilicate glass, molecular dynamics, structure, NMR-GIPAW

1 | INTRODUCTION

Boron-containing glasses find wide industrial and technological applications such as sealing glass, glass containers resistant to chemicals and heat, insulating fiber glasses, optical glasses and nuclear waste glasses as well as bioactive glasses.[1,2] Although there has been an upsurge in the development of borate and borosilicate based glasses, the majority of the glasses reported in the literature have been designed using the conventional "trial – and – error" approach. A notable example is given by the bioactive 13-93B3 bioactive glass, which has been essentially derived from a well-known silicate-based bioactive glass 13-93 by simply replacing SiO_2 with B_2O_3 with little other rationale or optimization. Improving upon this style of serendipitous composition design will require a deeper fundamental understanding of the compositional and structural drivers controlling the chemical durability of these glasses. Therefore, a new level of conceptual understanding about the compositional and structural dependence of dissolution behavior and other properties of boron-containing glasses is required that can be applied to attain a significant leap in the design of glasses suitable for specific applications. In the field of bioactive glasses, one major challenge that decelerates the design and development of boron-containing bioactive glasses with controlled corrosion behavior is the lack of reliable computational models to decipher the structural descriptors for these glasses which, upon convergence with the experimental data on glass dissolution, can be used to develop predictive Quantitative Structure-Property Relationship models.[3,4]

In the last decades, considerable achievements have been made in using classical molecular dynamics simulations to predict glass structure and properties.[5–8] However, exploring the structure of boron-containing glasses through atomistic simulations has been historically a challenge due to the complexity of boron-oxygen bonding (which is not only partially covalent but also allows the boron coordination in glass to change with composition as shown in Equations [1] and [2]) and its dependence on the thermal history of glass.[9] Therefore, it has been difficult to develop adequate B–O interatomic potentials.

$$1/2M_2O + B\emptyset_3 = M^+ + BO\emptyset_2^- \text{ (creation of NBO, as in silicates)} \quad (1)$$

$$1/2M_2O + B\emptyset_3 = M^+ + B\emptyset_4^- \left(\text{conversion of } B^{[III]} \text{ to } B^{[IV]}\right) \quad (2)$$

where M_2O refers to an alkali oxide, and Ø represents bridging oxygen atoms that are shared between adjacent structural borate units, B^{III} and B^{IV} represent BO_3 and BO_4 units, while NBO stands for non-bridging oxygen. The literature on borates and borosilicate glasses[10,11] suggest that the mechanism presented in Equation (2) is dominant when the ratio $R = [M_2O]/[B_2O_3] < 0.5$ whereas both mechanisms (Equations [1] and [2]) coexist for higher ratios.[12]

Until recently, no accurate and transferable interatomic potentials parameters were available in the literature to model boron-containing glasses, and previous classical MD simulations of borosilicate glasses provided structure only in partial agreement with experimental data.[13,14] Some of these limitations were overcome by the interatomic potential introduced by Kieu et al[15] and Inoue et al[16] that allowed reproducing the variations in coordination number of borate units as a function of composition owing to the direct dependence of atomic charges and boron parameters on the glass composition.[15] However, there are several shortcomings in the Kieu et al potentials which do not allow them to model the structure of borosilicate glasses over a broad composition space.[16] In the past 1 year, four new interatomic potentials parameters have been developed by—one each—by Wang et al[17] (hereafter referred as Bauchy potential), Deng and Du[18] (hereafter referred as Du potential), Stevensson et al[19] (hereafter referred as Edén potential) and by Pacaud et al.[20] The Bauchy and Du interatomic potentials rely on the rigid ionic model with pair potentials and partial charges whereas the Edén potential relies on the shell model potentials to describe ion polarization with formal charges on ions. Instead, the Pacaud potentials are based on the Polarizable Ion Model developed by Madden et al[21] in which at each ion a dipole polarizability and an induce dipole moment (determined minimizing the polarization energy term) are associated. Another distinction is that the Bauchy, Edén and Pacaud potentials have fixed charges and potential parameters, while the Du potential has a composition dependent parameter for B-O interactions to account for the composition dependence of the boron coordination changes with fixed partial atomic charges. These potentials generally exhibit good accuracy especially in borosilicate glass compositions investigated in the respective works.

Bauchy potential was originally validated against the fraction of four coordinated boron (hereafter referred as N_4), glass density and shear viscosity values of nine soda-lime borosilicate glasses of composition $15Na_2O$ 10CaO $(75 - x)$ B_2O_3 $xSiO_2$ where x varied between 0 and 75 mol%. In the studied compositional regime, the N_4 fractions and densities were very well reproduced with maximum relative error of about 6% and 2%, respectively.[17]

Deng and Du investigated the N_4 fraction and density of about 11 sodium borates and more than 100 sodium borosilicate glasses with wide ranges of R and K values, where $R = [M_2O]/[B_2O_3]$ and $K = [SiO_2]/[B_2O_3]$, showing that their composition dependent potentials can reproduce N_4 fraction and densities with average relative errors of 10 and 1%-2%, respectively. In glasses with $K = 1$ and 2, the maximum discrepancies were observed for glasses having R values close to

the $R_{max} = K/15 + 0.5$ value for which the maximum N_4 values were observed. In general, Du potentials slightly overestimate the fraction of BO_4 units in such compositions. On the contrary, in glasses with $K = 3$ and 4, the larger discrepancies were observed for glasses having $2 < R < 5$ and in such cases the simulated values slightly underestimate the experimental results.

As expected for rigid ionic models,[22] larger discrepancies were observed in the reproduction of silicon Q^n distributions. It is well known that to reproduce better medium-range structural features such as the Q^n distributions core-shell-based force fields such as the Edén potentials have be used, albeit they are computationally more expensive than the rigid ionic models.

Edén potentials were successfully used in their original work[19] to investigate composition-structure trends in 20 glass compositions over a broad composition space covering sodium borates (seven compositions), sodium borosilicates (seven compositions), soda-lime borophosphosilicates (six compositions) with different R, K and $f = \frac{100\times[B_2O_3]}{([SiO_2]+[B_2O_3])}$ values. Considering only borate and borosilicate glasses studied in the work, the average absolute relative error on the reproduction of the N_4 fraction was found to be 5.9%, which is within the limits of uncertainty and in agreement with Bauchy and Du results. However, an error of about 26% was found for the glass with composition $17.7Na_2O$ $13.5B_2O_3$ $68.8SiO_2$ (mol%) ($R = 1.31$ and $K = 5.1$) and an experimental N_4 fraction of 83%. Yu et al[23,24] have demonstrated good transferability of the Edén potentials subsequently in the investigation of several soda-lime borophosphosilicate glasses with different compositions from the ones used in the original paper. However, it should be noted that among the boron-containing glasses investigated by Edén's group in Ref.[19] only in 2 out of the 20 cases, the BO_4 is the dominating boron species.

Finally, the interatomic potential parameters developed by Pacaud et al[20] have been validated against neutron diffraction structure factors, N_4 fraction and density of five sodium borosilicate glasses with different R and K values. The average error for the prediction of N_4 value was 10.6% with a maximum error of about 26% for a glass with composition $34.5Na_2O$ $18.5B_2O_3$ and $47SiO_2$ mol% ($R = 1.86$ and $K = 2.54$). In this case, Pacaud potentials overestimate the fraction of BO_4 units. It is interesting to note that all the glasses studied by Pacaud et al present dominance of BO_4 units.

All the potentials mentioned above have been validated using different glass compositions and comparing the estimated N_4 fraction from MD with the one extracted from ^{11}B MAS-NMR spectra or the Dell-Bray model. However, with the recent development of density functional theory (DFT) methods to compute shielding[25] and electric field[26] gradient tensors in periodic systems, it is nowadays possible to directly compare simulated solid-state NMR spectra based on MD-derived glass structural models with the experimental counterparts in order to (a) validate models and thus interatomic potentials and computational procedures; (b) interpret experimental spectra; and (c) unravel correlations between NMR and structural parameters.[27–33]

In the present study, we have assessed the performance of the Bauchy, Du, and Edén interatomic potential models to reproduce the structure of a series of potentially bioactive sodium borosilicate glasses with composition $25Na_2O$–xB_2O_3–$(75 - x)SiO_2$ ($x = 0$, 18.4, 37.7, 56.25, and 75 mol%) with constant $Na_2O/(B_2O_3 + SiO_2) = 0.33$ for which the physical properties such as density and corrosion rate, and structural features such as ^{11}B NMR were reported by some of us.[9] The glass series was chosen because it encompasses different R (0.35-1.36) and K (0.365-3.076) values and thus, provides us an opportunity to explore a diverse boron environment with N_4 varying between 37% and 70%. Moreover, these compositions have not been investigated in any of the original articles describing the potentials,[17–19] therefore, making a good test case for ascertaining the validity of the three interatomic potentials. This task has been accomplished by comparing the ^{11}B, ^{29}Si, and ^{23}Na MAS-NMR spectra simulated using NMR parameters computed at the DFT-GIPAW level[25,27,34] on structural models containing up to 400 atoms generated through MD simulations with the three interatomic potential models with the experimental counterparts. The structural variations of the models after DFT optimizations have been deeply analyzed in terms of average bond lengths and angles, coordination numbers and silicate Q^n speciation (Q is a quaternary species, and n is the number of bridging oxygens around it).

2 | COMPUTATIONAL DETAILS

2.1 | Generation of glass models

A series of sodium borosilicate glasses reported in our previous study with composition $25Na_2O$–xB_2O_3–$(75 - x)SiO_2$ ($x = 0$, 18.4, 37.5, 56.25 and 75 mol%) with constant $Na_2O/(B_2O_3 + SiO_2) = 0.33$ have been generated through classical MD simulations by using the melt-quench approach.[5] These glasses have been labeled as Bx hereafter, where x refers to the molar concentration of B_2O_3. We had investigated the impact of thermal history on the structure and dissolution behavior of these glasses where the melts were quenched using two different methods, that is, (a) quenching between two copper plates; and (b) quenching on a metallic plate followed by annealing to minimize the residual stress. Since the MD glasses are generated using ultrafast quenching rates, we have used the experimental data of the glasses produced by quenching the melts between two copper plates. Furthermore, we have used the experimentally analyzed glass compositions (instead of the batched compositions) and experimentally measured density values of glasses (as reported in Table 1) in the present study.

TABLE 1 Glass compositions and densities used in MD simulations

Glass	Na_2O	B_2O_3	SiO_2	*R*	*K*	*d* (g/cm3)
B-0	25.1	—	74.9	—	—	2.331
B18.4	25.1	18.4	56.5	1.364	3.071	2.423
B37.5	25.1	37.2	37.7	0.675	1.013	2.386
B56.25	24.8	55.1	20.1	0.450	0.365	2.292
B-75	25.9	74.1	—	0.350	—	2.183

Models containing 337-410 atoms were used to compute ^{11}B, ^{29}Si, and ^{23}Na MAS-NMR parameters and simulate solid-state MAS-NMR spectra. Three replicas for each composition have been generated to improve statistics of MAS-NMR data. The number of atoms in the generated models has been reported in Table S1.

Three recently developed force fields parameters especially devised for boron-containing multicomponent glasses have been used and tested in this work. As mentioned earlier, the Bauchy and Du potentials are based on the rigid ions with partial charges that interact through pairwise Buckingam potentials:

$$U_{ij}(r)=\frac{q_i q_j e^2}{r}+A_{ij}e^{-r/\rho_{ij}}+\frac{C_{ij}}{r^6} \tag{3}$$

Bauchy and Du potentials differ with regard to the values of charges ($q_O=-0.945$ for Bauchy potentials and $q_O=-1.2$ for Du potentials) and the fact that whereas the former set uses B-O parameters independent by the glass compositions while the latter set has the repulsive A parameter for B-O dependent on the glass composition as follows:

$$A_{B-O}=\begin{cases} A_1+t_1\times\left(R_{\max}-\left(R_{\max}-N_4\right)^2/R_{\max}\right)+t_2\times K^2 & R\le R_{\max} \\ A_2+t_3\times R_{\max}\times N_4/R & R>R_{\max}\end{cases} \tag{4}$$

where A_1, A_2, t_1, and t_2 are empirical parameters with values of 11900.0, 12525.0, 4350.0, and 85.0 eV, respectively. *R* and *K* values are two ratios determined by the composition, equal to $[Na_2O]/[B_2O_3]$ and $[SiO_2]/[B_2O_3]$, respectively. N_4 is the predicted fraction of fourfold coordinated boron of the interested glass composition based on the Dell, Bray, and Xiao (DBX) model.[35] The DBX model can generally predict the N_4 values in a wide composition space based on *R* and *K* values. The R_{max} value is the *R*-value at which N_4 reaches a maximum value in the DBX model and is equal to $K/16 + 0.5$. Finally, the t_3 value is derived through the following equation:

$$t_3=\frac{\left(A_1+t_2\times K^2-A_2\right)}{R_{\max}}+t_1 \tag{5}$$

To avoid the Buckingham catastrophe at short interatomic distances a repulsive term of the form D_{ij}/r^{12} and a splice correction of the form $\frac{B_{ij}}{r_{ij}^n}+D_{ij}\cdot r_{ij}^2$ have been applied at small *r* for the Bauchy and Du potentials, respectively. The Bauchy and Du parameters for all the atomic pairs used have been included in Tables S2 and S3 of the supplementary materials, respectively.

The Edén potentials are based on the shell model[36] to account for ion polarization where the total charge Z of the oxygen ions is split between a core (of charge Z + Y) and a massless shell (of charge −Y) which are coupled by a harmonic spring. Besides the damped harmonic interaction with the corresponding core, the oxygen shells interact with each other and with Si, B, and Na cations through an extended Buckingham function of the type:

$$U_{ij}(r)=A_{ij}e^{-\frac{r}{\rho_{ij}}}-\frac{C_{ij}}{r^6}\left[1-e^{-\left(\frac{r}{4.3\rho_{ij}}\right)^6}\right]+\frac{D_{ij}}{r^{12}} \tag{6}$$

whereas coulombic forces act between all species which bear full formal charges. A three-body truncated harmonic potential is used to control the intra-tetrahedral O-Si-O angles during dynamics.

$$U\left(\theta_{jik}\right)=\frac{k_{jik}}{2}\left(\theta_{jik}-\theta_{jik,0}\right)^2 e^{-\frac{\left(r_{ij}^8+r_{jk}^8\right)}{\rho_{jik}^8}} \tag{7}$$

The potential parameters have been reported in Tables S4 and S5 of the supporting information.

The leap-frog algorithm encoded in the DL_POLY2.14 package[37] has been used to integrate the equation of motions with a time step of 0.2 fs for the Edén potentials, that is, small enough to control the high-frequency motion of the core-shell spring during MD simulations[38] and 2 fs for the Bauchy and Du potentials. The initial configurations were generated by placing randomly the number of atoms in a cubic box, whose dimension allows the experimental density to be reproduced.

Two slightly different cooling procedures have been used for the different interatomic potentials. For the simulations adopting the Bauchy and Edén potentials, the systems were heated and held at 3200 K for 100 ps in the NVT ensemble ensuring a suitable melting of the samples. The liquids were then cooled to 300 K at a nominal cooling rate of ~5 K/ps. The resulting glass structures were subjected to a final equilibration run of 200 ps.

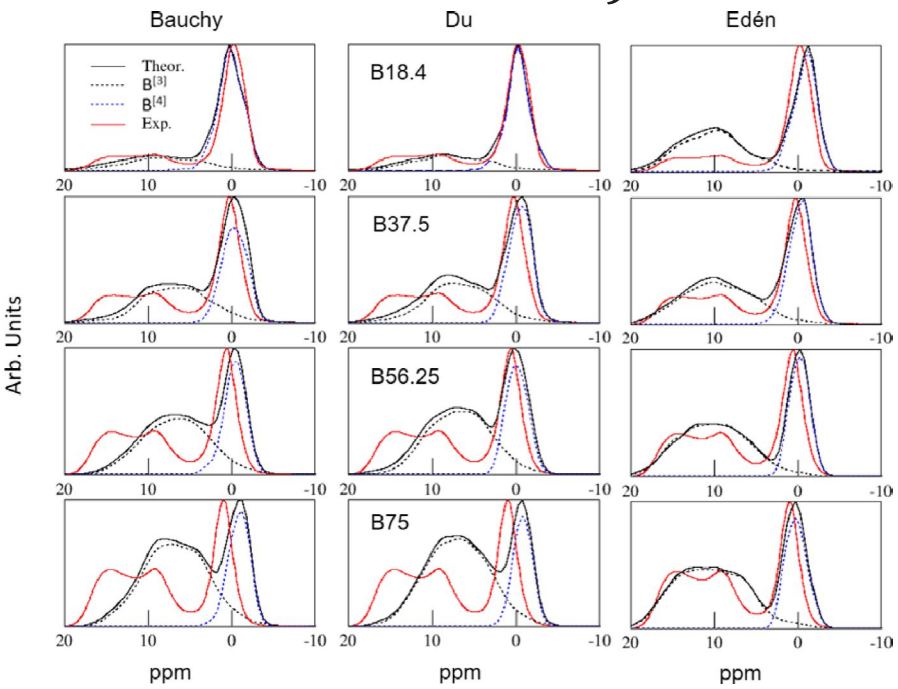

FIGURE 1 ^{11}B MAS NMR of the investigated borosilicate glasses computed using structural models generated by using Bauchy (left), Du (middle), and Edén (right) potentials. The experimental spectra are reported in red. The magnetic field is 11.7T. Spectra have been broadened using Gaussian functions with HWHM = 100 Hz. HWHM, half-width at half-maximum

In the case of the simulations with Du potentials, the system was heated to 6000 K, equilibrated for 100 ps, and subsequently cooled down continuously from 6000 to 300 K in 1140 ps with a nominal cooling rate of 5 K/ps. Relaxation at 300 K under NVT ensemble was performed for 100 ps, which is followed by another 100 ps of equilibration at constant energy (NVE), and 50 ps of data production was performed at 300 K. All the simulations were carried out using the NVT ensemble with Berendsen thermostat[39] with frictional constants set to 0.4 ps.

Coulomb interactions have been calculated by the Ewald summation method with a cutoff of 8 Å for all the potentials whereas short-range cutoff values of 5.5 and 7.5 Å have been used for the rigid ionic and shell model potentials, respectively.

2.2 | DFT-NMR calculations and simulation of NMR spectra

Chemical shielding and EFG tensors were computed with the NMR-CASTEP[34] DFT code using the GIPAW[25] and PAW[26] algorithms, respectively. The generalized gradient approximation PBE[40] functional was employed, and the core-valence interactions were described by ultrasoft pseudopotentials generated on the fly. For ^{17}O, the 2s and 2p orbitals were considered as valence states with a core radius of 1.3 a.u.; for ^{29}Si, a core radius of 1.8 a.u. was used with 3s and 3p valence orbitals, for ^{23}Na, a core radius of 1.3 a.u. was used with 2s, 2p, and 3s valence orbitals while for ^{11}B, a core radius of 1.405 a.u. was used with 2s and 2p valence states. For the PAW and GIPAW calculations we used two projectors in each s and p angular momentum channel for O and B, and in the s, p, and d channel for Si and Na.

Before computing the NMR parameters, constant volume geometry optimizations of the models generated with MD using classical potentials were performed at the Γ point. Wave functions were expanded in plane waves with the kinetic energy cutoff of 610 eV, and this cutoff has been demonstrated to be large enough to reach energy, and NMR chemical shift converged values.

Furthermore, to fix the ^{29}Si, ^{11}B, and ^{23}Na δ scale the values of 322.1,[41] 95.05,[42] and 554.05[29] have been used for σ_{ref}. The experimentally determined quadrupolar moment, eQ, of 40.59 and 104 mB were used for the ^{11}B and ^{23}Na atoms.[43] However, since the existing literature demonstrated that with these values the computed C_Q constant results were overestimated, we post-scaled the ^{11}B and ^{23}Na C_Q values by the values 0.842 and 0.46, respectively, as was suggested in previous works.[29,42]

The simulation of the solid-state MAS spectra from the CASTEP outputs has been carried out using the software SoSNMR.[44] For each atomic site i, the powder line shape, $I_i(v)$, for a rotor spinning at infinity frequency at a particular angle θ_R is computed by averaging upon the (φ, θ) angles using the following equation:

$$I_i(v) = \sum_{m=-I+1}^{I} \rho(m) \int_0^{\pi} \int_0^{2\pi} G\left(v - v_{m,m-1}(\phi,\theta)\right) \sin\theta \, d\theta d\phi \qquad (8)$$

where $\rho(m) = I(I+1) - m(m-1)$ are the weighting factors for the satellite intensities[45] and $G(v)$ is a Gaussian or Lorentzian broadening function and then co-added to yield the final NMR spectra $I(\vec{v}) = \sum_i I_i(\vec{v})$. Gaussian broaden-

ing functions with half-width at half-maximum of 100 Hz per each site has been used in this work. The conventional grid point method of integrating over the Euler angle space was used.[46]

3 | RESULTS AND DISCUSSIONS

In this section, we compare the computed ^{11}B, ^{29}Si, and ^{23}Na MAS-NMR spectra of the glass structural models generated with the three potentials with the experimental ones. The cation environments in glasses before and after DFT geometry optimizations were also compared to have a feeling of the differences between the classical MD and DFT levels of relaxations. When available, structural data has also been compared with experimental counterparts.

3.1 | Boron environment

Figure 1 reports the comparison between the ^{11}B MAS NMR spectra simulated using structural models generated with the Bauchy, Du and Edén potentials and the experimental ones for the B18.4, B37.5, B56.25, and B75 glasses. In general, a good agreement is observed denoting that the DFT refinement of the MD-generated structural models reproduces the boron environment fairly well. In particular, the areas underlying the $BO_3 \equiv B^{[3]}$ and $BO_4 \equiv B^{[4]}$ peaks observed respectively at 10-20 ppm and around 0 ppm are in nice agreement for B18.4 and B37.5 glasses generated with Bauchy and Du potentials denoting a good repartition between the $B^{[3]}$ and $B^{[4]}$ species in the models. The agreement with experiments is worse for the B56.25 and B75 glasses. It is worth noting that the shape and the broadening of the $B^{[4]}$ peak are very well reproduced for all the glasses and all potentials whereas some discrepancies are observed for that of the $B^{[3]}$ species. In particular, the $B^{[3]}$ peak of the simulated spectra of the models generated with the Bauchy and Du potentials is shifted to less positive chemical shifts when compared with the corresponding experimental results. In the previous work, a shift to less negative chemical shifts was attributed to the presence of non-ring $B^{[3]}$ units.[47] A better agreement in this respect is observed for the models generated using Edén potentials where the $B^{[3]}$ and $B^{[4]}$ peaks exhibit a good overlap with the experimental spectra overlap. However, even if the $B^{[3]}$ peak position is well reproduced the shape with a double peak which is usually observed for triborate and pentaborate superstructural units[42] is not.

The analysis of our structural models revealed that boroxol rings are absent in all the models. However, whereas in the Bauchy and Du models no $B^{[3]}$ species are present in three membered rings, a small amount of $B^{[3]}$ species in three membered rings are found in the Edén's models.

In particular, 1.4% of the total boron atoms are found as $B^{[3]}$ species in three-membered rings (composed by both $B^{[3]}/B^{[4]}$ and Si) for B18.4 and B37.5 glasses whereas 6.2 and 4.9% of the total boron atoms are found as $B^{[3]}$ species in 3-m rings for the B56.25 and B75 glasses. In the last two cases, the 3-m rings are constituted by only boron ($B^{[3]}$ and/or $B^{[4]}$) atoms resembling triborate or pentaborate units, but their amount is not sufficient to reproduce

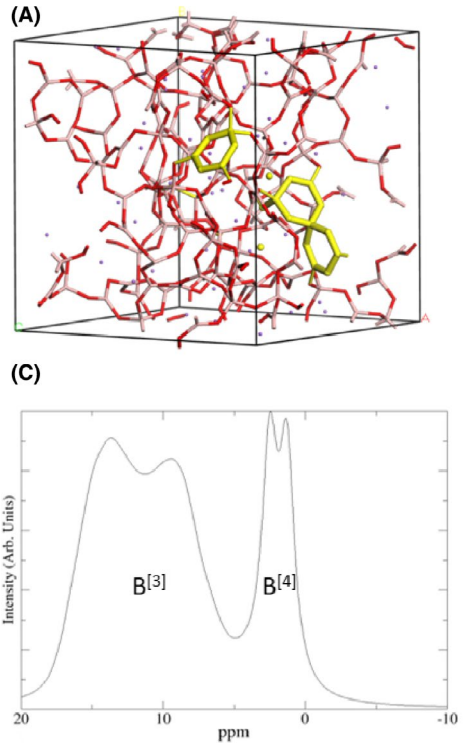

NMR parameters	$B^{[3]}$	$B^{[4]}$
δ_{iso} (ppm)	17.6-18.0	3.0
C_Q (MHz)	2.44-2.52	0.42
η_Q	0.21-0.33	0.60

FIGURE 2 (A) Structural model of the B75 glass generated with Edén potentials with triborate or dipentaborate units highlighted in yellow. (B) Structure of the sodium dipentaborate crystal optimized at the DFT level and (C) its simulated ^{11}B MAS NMR spectra (B0 = 11.7 T). The NMR parameters computed for the $B^{[3]}$ and $B^{[4]}$ species are also reported. Spectrum has been broadened using Gaussian functions with HWHM = 100 Hz. HWHM, half-width at half-maximum. DFT, density functional theory

the peak shape. Some of these units are shown in Figure 2 together with the ^{11}B MAS NMR spectra computed for the sodium dipentaborate crystal that shows the typical $B^{[3]}$ double peak of pentaborate units.

To understand the reasons behind the differences in the reproduction of the spectra using Bauchy and Du models that provides very similar results and the ones obtained using Edén models we have analyzed the structures before and after DFT optimizations.

Table 2 reports the fraction of N_4 species in the investigated glasses computed with the Bauchy, Du, and Edén interatomic potentials parameters along with the fractions estimated using the BDX model and those extracted from ^{11}B MAS NMR experiments. The experimental data shows that the fraction of N_4 decreases from 0.697 for the glass B18.4 to 0.374 for the glass B75. The data has been satisfactorily reproduced by the BDX model and to a lesser extent by the MD simulations. It is worth to highlight that since MD data are computed on relative small boxes, the uncertainties are about ±0.05 (B18.4 and B37.5 glasses) and 0.03 (for B56.25 and B75 glasses) units. Based on these uncertainties we can state that all the interatomic potentials well reproduce the N_4 fraction for B37.5, B56.25, and B75 glasses. In general, after DFT geometry optimization the N_4 fraction decreases for the glasses produced with Bauchy and Du potentials whereas smaller variations are observed for Edén's models. Among the glasses, the larger discrepancies are observed for B18.4 for which the N_4 fraction is overestimated by Bauchy and Du and underestimated by Edèn's potential. Interestingly, in all cases, the DFT optimization changes the values towards the experimental values.

A large underestimation remains of the N_4 values for B18.4 using the Edén potentials. The comparison between the average $B^{[3]}$-O and $B^{[4]}$-O bond distances computed at the MD and DFT level is reported in Table 3.

Bauchy potentials provide average $B^{[3]}$-O distances of about 1.41 Å and $B^{[4]}$-O distances of about 1.49 Å; Du potentials provide distances respectively of about 1.43-1.44 Å and 1.54-1.55 Å whereas Edén potentials provide distances of about 1.35-1.36 Å and 1.42 Å, respectively.

After DFT optimization, the average $B^{[3]}$-O bond length is about 1.37-1.38 Å for Edén models and 1.38-1.39 for Bauchy and Du models while the average $B^{[4]}$-O bond length is about 1.47-1.48 Å for Edén models and 1.49-1.50 for Bauchy and Du models. In all cases, the $B^{[3]}$-O and $B^{[4]}$-O distances differ of about 0.1 Å.

These distances are similar to those found by Petesseau et al[48] by using AIMD simulations on a sodium borosilicate glass with composition $3Na_2O\ B_2O_3\ 6SiO_2$ for which the $B^{[3]}$-O and $B^{[4]}$-O bond lengths were found to be 1.37 and 1.47 Å, respectively.

The DFT data are also in excellent agreement with the bond lengths of 1.37 and 1.47 Å for $B^{[3]}$ and $B^{[4]}$ species determined using neutron diffraction experiments on borate glasses.[49]

These data reveal that in general Bauchy and Du potentials provides longer B-O distances concerning DFT calculations whereas Edén potentials underestimate the $B^{[4]}$-O bond lengths and thus the differences between $B^{[3]}$-O and $B^{[4]}$-O bond lengths.

However, after geometry optimization at the DFT level, the boron environment is pretty the same for all the generated models. This means that the differences in the simulated spectra must be related to other medium-range structural characteristics.

Larger discrepancies are observed for the average inter-tetrahedral angles B-O-T between the three models before and after geometry optimization.

These data are reported in Table 4. Bauchy, Du, and Edén models present $B^{[3]}$-O-Si ($B^{[4]}$-O-Si) average angles of about 144-147°(141-144°), 146-152° (148-150), and 130-135° (133°), respectively. After DFT optimizations, these angles reduce to 137-141° (137-139°), 137-144° (144-145°), and 131-135° (132-135°) for Bauchy, Du, and Edén models.

These data confirm that Bauchy and Du potentials overestimate the inter-tetrahedral angles and in most of the cases DFT optimization reduces it by several degrees providing in both cases similar final values. On the contrary, Edén's models provide much narrower angles that are only slightly varied by DFT optimizations. In general, Bauchy and Du potentials produce $B^{[3]}$-O-Si angles larger than $B^{[4]}$-O-Si whereas both Edén and DFT optimized models provide quite similar angles. Similar consideration can be done for $B^{[3]}$-O-$B^{[3]}$, $B^{[3]}$-O-$B^{[4]}$, and $B^{[4]}$-O-$B^{[4]}$ angles, which are also reported

TABLE 2 Fraction of N_4 species in the simulated glasses using the Bauchy, Du, and Edén potentials before (in parenthesis) and after DFT geometry optimization. The N_4 fractions estimated with the Dell and Bray model and extracted from ^{11}B NMR spectra are also reported

	B18.4	B37.5	B56.25	B75
Bauchy	0.73 (0.78)	0.51 (0.56)	0.37 (0.43)	0.30 (0.34)
Du	0.70 (0.77)	0.47 (0.51)	0.36 (0.42)	0.27 (0.32)
Edén	0.50 (0.49)	0.47 (0.46)	0.40 (0.39)	0.36 (0.33)
Dell and Bray	0.69	0.56	0.45	0.35
Exp.	0.70	0.57	0.44	0.37

Abbreviation: DFT, density functional theory.

TABLE 3 Average bond distances of the simulated glasses using the Bauchy, Du, and Edén potentials computed after MM (in parenthesis) and after DFT geometry optimization

		B0	B18.4	B37.5	B56.25	B75
Na-O	Bauchy	2.386 (2.547)	2.413 (2.569)	2.378 (2.511)	2.367 (2.536)	2.419 (2.548)
	Du	2.359 (2.447)	2.418 (2.473)	2.436 (2.574)	2.454 (2.492)	2.431 (2.516)
	Edén	2.397 (2.386)	2.419 (2.470)	2.402 (2.451)	2.433 (2.450)	2.399 (2.465)
$B^{[3]}$-O	Bauchy	—	1.389 (1.418)	1.387 (1.413)	1.384 (1.414)	1.384 (1.413)
	Du	—	1.389 (1.434)	1.387 (1.435)	1.385 (1.439)	1.385 (1.428)
	Edén	—	1.381 (1.360)	1.376 (1.353)	1.376 (1.352)	1.375 (1.356)
$B^{[4]}$-O	Bauchy	—	1.491 (1.488)	1.493 (1.491)	1.494 (1.491)	1.491 (1.490)
	Du	—	1.498 (1.549)	1.497 (1.541)	1.499 (1.543)	1.491 (1.535)
	Edén	—	1.476 (1.403)	1.479 (1.421)	1.477 (1.423)	1.474 (1.422)
Si-O	Bauchy	1.636 (1.642)	1.637 (1.642)	1.639 (1.643)	1.639 (1.642)	—
	Du	1.632 (1.611)	1.635 (1.612)	1.635 (1.609)	1.641 (1.611)	—
	Edén	1.631 (1.641)	1.626 (1.638)	1.626 (1.644)	1.628 (1.650)	—
Si-NBO	Bauchy	1.582 (1.616)	1.594 (1.630)	1.593 (1.615)	1.568 (-)	—
	Du	1.588 (1.567)	1.595 (1.567)	1.584 (1.603)	1.574 (1.588)	—
	Edén	1.583 (1.605)	1.580 (1.590)	1.584 (1.604)	—	—
Si-BO	Bauchy	1.647 (1.646)	1.640 (1.643)	1.641 (1.644)	1.642 (1.645)	—
	Du	1.642 (1.621)	1.641 (1.617)	1.638 (1.611)	1.646 (1.612)	—
	Edén	1.641 (1.649)	1.630 (1.641)	1.627 (1.645)	1.628 (1.650)	—

Abbreviation: DFT, density functional theory.

in Table 4. These angles are overestimated by Bauchy and Du potentials and better reproduced by Edén potentials. As before, the DFT data are in nice agreement with previous AIMD simulations on sodium borosilicate glasses performed by Pedesseau et al.[48]

Therefore, the quality of the ^{11}B MAS NMR spectra computed on the Bauchy and Du models is essentially the same because of the similarity between the B-O-T angles whereas the better shift found for $B^{[3]}$ peak with the Edén models is due to the smaller angles and narrower bond angle distributions (see Figure S1 of the ESI) with respect to the other models.

Indeed, as shown in Figure 3 and reported in previous investigations there is a negative correlation with the isotropic chemical shift for the B-O-T angles of $B^{[3]}$ species.

Table 5 reports the ^{11}B NMR parameters (δ_{iso}, C_Q and η_Q) of the $B^{[3]}$ and $B^{[4]}$ species as a function of the second coordination sphere, that is, the number of Si and B connected to the central boron atom and their relative populations. Figure 4 reports the average ^{11}B δ_{iso} and C_Q values against the number of boron atoms in the second coordination sphere computed by using all the glass models generated with the three potentials. The δ_{iso} values for the Bauchy and Du models are very similar among them ranging from ~11 ppm to ~18ppm for $B^{[3]}$ species whereas the values observed for the Edén models are slightly higher because of the smaller B-O-T average angles. Instead, the isotropic chemical shift for $B^{[4]}$ species ranges between ~−4 ppm and ~4-5 ppm for the Bauchy and Du models denoting once again that after DFT optimization the short-range order of boron in the two models is essentially the same. Narrower ranges between −1.7 and 0.9 ppm are observed for Edén models.

For both species, the higher δ_{iso} are observed for boron atoms having one non-bridging oxygen which are, however, present in very small amounts (between 0.01 for B75 and 0.17 for B18.4 with Edén potentials). The results for all the glasses and force fields show that the isotropic chemical shift slightly increases with the amount of B in the second coordination sphere for $B^{[3]}$ species.

For example, δ_{iso} increases from 11.3 ppm for boron atoms surrounded by three silicon atoms (zero boron atoms) to 11.9 ppm, 12.3 ppm and 13.1 ppm for boron atoms connected to two silicon atoms (one boron), one silicon (two boron) and zero silicon atoms (three boron atoms), respectively for the B37.5 glass generated with Bauchy potentials. Figure 4 and Table 5 show that this trend is not observed for $B^{[4]}$ species, probably because the isotropic chemical shift distribution is much narrower.

Regarding C_Q values, they range between 2.4 and 2.9 MHz for $B^{[3]}$ species (C_Q increases with the number of boron atoms in the second coordination sphere for Edén models and decreases for Bauchy and Du models) and between 0.4 and 0.8 MHz for $B^{[4]}$ species. In the latter case, the largest values are observed for species with high B/Si intermixing in

TABLE 4 Average bond angles of the simulated glasses using the Bauchy, Du, and Edén potentials computed after MM (in parenthesis) and after DFT geometry optimization

		B0	B18.4	B37.5	B56.25	B75
Si-O-Si	Bauchy	145.0 (149.2)	145.6 (147.9)	141.7 (143.6)	147.8 (147.3)	—
	Du	146.7 (155.5)	144.0 (150.1)	145.9 (148.9)	140.0 (146.4)	—
	Edén	144.2 (143.2)	142.3 (144.5)	142.4 (145.0)	136.3 (138.3)	—
Si-O-$B^{[3]}$	Bauchy	—	136.7 (146.5)	138.9 (146.6)	141.4 (144.3)	—
	Du	—	137.3 (146.4)	144.1 (152.1)	142.5 (150.6)	—
	Edén	—	130.6 (129.8)	134.9 (132.0)	131.2 (134.6)	—
Si-O-$B^{[4]}$	Bauchy	—	136.9 (141.1)	138.6 (144.4)	138.8 (141.6)	—
	Du	—	144.8 (149.2)	144.3 (148.1)	144.4 (150.4)	—
	Edén	—	134.7 (133.4)	132.5 (133.2)	132.9 (133.6)	—
$B^{[4]}$-O-$B^{[4]}$	Bauchy	—	133.0 (141.3)	137.5 (147.2)	138.8 (151.1)	143.3 (152.8)
	Du	—	144.3 (146.9)	144.1 (151.1)	140.2 (144.4)	134.9 (152.1)
	Edén	—	140.0 (132.8)	119.1 (126.3)	126.7 (126.9)	125.9 (122.2)
$B^{[4]}$-O-$B^{[3]}$	Bauchy	—	141.3 (145.4)	140.9 (151.8)	141.1 (148.1)	138.2 (150.8)
	Du	—	137.3 (138.1)	139.5 (143.7)	136.0 (143.4)	138.8 (146.1)
	Edén	—	130.8 (130.3)	126.3 (126.1)	127.2 (127.0)	123.5 (123.8)
$B^{[3]}$-O-$B^{[3]}$	Bauchy	—	—	142.4 (154.6)	144.3 (156.0)	142.6 (156.1)
	Du	—	153.0 (178.0)	140.5 (151.3)	142.7 (151.9)	140.8 (155.1)
	Edén	—	—	124.4 (123.6)	126.0 (125.0)	126.0 (124.7)

Abbreviation: DFT, density functional theory.

the second coordination sphere for Bauchy and Du models. Finally, no particular trends are observed for the asymmetry parameter η_Q.

In Table S6 of the ESI, the NMR parameters of $B^{[3]}$ and $B^{[4]}$ species have been investigated as a function of the number of $B^{[3]}$ and $B^{[4]}$ species to determine, which is the effect of the boron speciation in the second coordination sphere.

In general, the results using Edén potentials (the only ones discussed here since it better reproduces the T-O-T angles) show contrasting trends depending on the total number of boron atoms in the second coordination sphere. In particular, regarding the isotropic chemical shifts trends, we observe that $\delta_{iso}\left(B^{[3],SiB3B4}\right) < \delta_{iso}\left(B^{[3],SiB4B4}\right)$, $\delta_{iso}\left(B^{[3],3B3}\right) < \delta_{iso}\left(B^{[3],B3B3B4}\right) < \delta_{iso}\left(B^{[3],B3B4B4}\right) < \delta_{iso}\left(B^{[3],B4B4B4}\right)$ for $B^{[3]}$ species whereas for $B^{[4]}$ species the trends are $\delta_{iso}\left(B^{[4],3SiB3}\right) > \delta_{iso}\left(B^{[4],3SiB4}\right)$, $\delta_{iso}\left(B^{[4],2SiB3B3}\right) < \delta_{iso}\left(B^{[4],2SiB3B4}\right)$ and $\delta_{iso}\left(B^{[4],4B3}\right) < \delta_{iso}\left(B^{[4],4B4}\right)$. That is, for $B^{[3]}$ species the substitution of $B^{[3]}$-O-$B^{[3]}$ bonds by $B^{[3]}$-O-$B^{[4]}$ bonds leads to an increase in the isotropic chemical shift. This happens also for $B^{[4]}$ species at the exception of $B^{[4]3SiB}$ and $B^{[4]}$Si3B species for which a clear trend is not distinguishable.

Regarding the quadrupolar coupling constants, we observed that: for $B^{[3]}$ species $C_Q\left(B^{[3],SiB3B3}\right) > C_Q\left(B^{[3],SiB3B4}\right) > C_Q\left(B^{[3],SiB4B4}\right)$ and $C_Q\left(B^{[3],3B3}\right) = C_Q\left(B^{[3],B3B3B4}\right) = C_Q\left(B^{[3],B3B4B4}\right) < C_Q\left(B^{[3],3B4}\right)$ whereas for $B^{[4]}$ species the trends are $C_Q\left(B^{[4],3SiB3}\right) < C_Q\left(B^{[4],3SiB4}\right)$, $C_Q\left(B^{[4],2SiB3B3}\right) < C_Q\left(B^{[4],2SiB4B4}\right)$ and $C_Q\left(B^{[4],4B3}\right) < C_Q\left(B^{[4],4B4}\right)$. No clear trends are observed for the asymmetry parameter.

3.2 | Silicon environment

Figure 5 reports the comparison between the ^{29}Si MAS NMR computed using the Bauchy, Du, and Edén structural models of the B0-B56.25 glasses and the experimental counterparts.

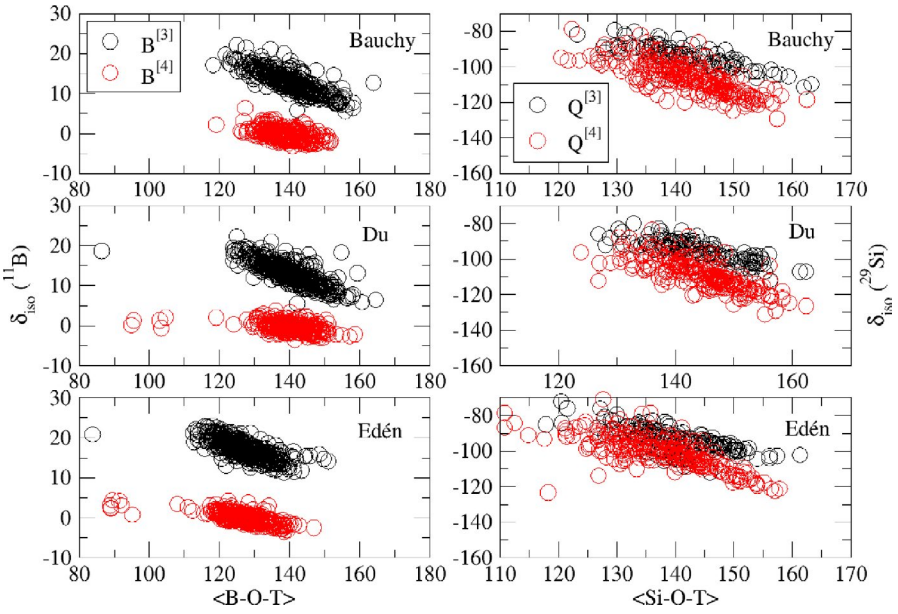

FIGURE 3 Correlations between δ_{iso} of ^{11}B (^{29}Si) with the average B-O-T (Si-O-T) angle for the three models

The simulated spectra using the Bauchy and Du potentials do not well reproduce the experimental ones regarding both the peak positions and shapes whereas Edén's models lead to spectra narrower and more in agreement with the experimental ones. The spectra of the Bauchy and Du models are shifted of more than 10-20 ppm to more negative isotropic chemical shifts depending on the glass. The spectra reproduced worst is the one of the B0 glass whose Q^n distribution is badly reproduced by both the rigid ionic potentials.

The Si Q^n species distributions before and after DFT geometry optimizations are reported in Table 6 and compared with the distributions reported in Ref.[9], which have been calculated from a combination of ^{11}B MAS NMR analyzed glass compositions and the calculated fraction of sodium as a network modifier. A binomial distribution of Q^3 and Q^4 species have been assumed for B0 to B37.5 glasses but whereas the Q^3 species are dominant (67.1%) in the B0 glass the substitution of boron for silicon increases the reticulation of the glass network which becomes dominated by Q^4 species. B56.25 glass was assumed 100% Q_4 due to complete Na consumption as a charge compensator for BO_4 units.

Firstly, it is worth to highlight that, differently from the short-range cation environments; the Q^n distributions do not change after DFT optimization. The structure of the B0 glass produced by the Bauchy and Du potentials is dominated by Q^3 (43% for Bauchy and 46% for Du model) and Q^4 (about 45% for both models) species in equal amount. As expected, Edén potentials provide structures dominated by Q^3 species (56%) and Q^4 species (37%) in better agreement with the estimated distributions in Ref.[9] A better agreement is also observed for the other glasses.

However, a little more surprising is the disagreement found for the B18.4 and B37.5 glasses since the Q^n species distributions in the MD-derived glasses with Bauchy and Du potentials are more similar to those reported in Ref.[9]

Since previous works[27,31,41,50,51] showed that the computed isotropic chemical shifts at the PBE-GIPAW level are within 1-2 ppm of the experimental ones and Edén models well reproduce the peak positions the large shift observed for Bauchy and Du models should not be attributed to wrong values of σ_{ref} or errors in the DFT calculations but rather to deficiencies in the structural models.

Table 3 suggests that such deficiencies are not related to the local environment of silicon since after DFT optimizations all the models have similar Si-O, Si-NBO, and Si-BO distances of 1.62-1.64 Å, 1.58-1.59Å, and 1.63-1.64 Å, respectively.

In general, after DFT optimization the Si-NBO distances decreases of 0.03 Å for Bauchy and of 0.02 Å for Edén models and increases of 0.02 Å for Du models. The Si-BO distances do not change for Bauchy models; it increases by 0.02 Å for Du and decreases of 0.01/0.02 Å for Edén models. Therefore, all potentials well reproduce Si-O distances with respect to DFT calculations.

As observed for boron above, huge changes are observed for Si-O-T angles (T = Si, $B^{[3]}$, and $B^{[4]}$) after DFT optimizations and between the potentials models. Bauchy and Du potentials provide larger average angles concerning Edén potentials that are only slightly varied by DFT optimizations.

Figure S1 of the ESI, which reports the Si-O-T bond angles distributions for systems containing 10 000 atoms, shows that the rigid ionic models provide also quite broad distributions.

Since a negative correlation is known for the isotropic chemical shift of silicon with the average Si-O-T angles (T = Si or B) as also evidenced in Figure 3, the δ_{iso} of ^{29}Si

TABLE 5 NMR parameters of $B^{[3]}$ and $B^{[4]}$ species for the investigated glasses as a function of the second coordination sphere. Only species with pop ≥ 0.02 have been tabulated

		B18.4				B37.5				B56.25				B75			
		pop	δ_{iso}	C_Q	η_Q	pop	δ_{iso}	C_Q	η_Q	pop	δ_{iso}	C_Q	η_Q	pop	δ_{iso}	C_Q	η_Q
Bauchy models																	
$B^{[3]}$	3Si	0.05	11.6	2.5	0.2	0.02	11.3	2.6	0.1	—	—	—	—	—	—	—	—
	2Si1B	0.08	12.8	2.5	0.3	0.14	11.9	2.5	0.2	0.03	12.6	2.5	0.3	—	—	—	—
	1Si2B	—	—	—	—	0.18	12.3	2.5	0.3	0.25	12.5	2.5	0.3	—	—	—	—
	3B	—	—	—	—	0.06	13.1	2.4	0.2	0.29	12.4	2.4	0.3	0.65	12.6	2.5	0.3
	2Si1NBO	0.08	17.1	2.5	0.7	—	—	—	—	—	—	—	—	—	—	—	—
$B^{[4]}$	4Si	0.36	−0.1	0.5	0.6	0.03	−0.7	0.4	0.6	—	—	—	—	—	—	—	—
	3Si1B	0.24	5.2	0.6	0.5	0.09	0.1	0.6	0.5	—	—	—	—	—	—	—	—
	2Si2B	0.07	1.7	0.9	0.5	0.17	−0.3	0.7	0.6	0.05	0.2	0.5	0.7	—	—	—	—
	1Si3B	—	—	—	—	0.15	−0.3	0.6	0.6	0.18	−4.0	0.6	0.6	—	—	—	—
	4B	—	—	—	—	0.03	0.6	0.7	0.7	0.13	−0.3	0.7	0.6	0.30	−0.6	0.6	0.7
Du models																	
$B^{[3]}$	3Si	0.07	12.3	2.5	0.1	—	—	—	—	—	—	—	—	—	—	—	—
	2Si1B	0.07	15.0	2.6	0.3	0.12	12.1	2.5	0.2	0.02	12.2	2.5	0.3	—	—	—	—
	1Si2B	0.05	11.8	1.2	0.1	0.21	12.5	2.5	0.3	0.21	12.6	2.5	0.3	—	—	—	—
	3B	—	—	—	—	0.07	13.2	2.4	0.2	0.35	12.7	2.5	0.3	0.65	12.5	2.5	0.3
	2Si1NBO	0.07	15.8	2.5	0.6	—	—	—	—	—	——	—	—	—	—	—	—
$B^{[4]}$	4Si	0.22	−0.6	0.4	0.6	0.03	−1.1	0.3	0.6	—	—	—	—	—	—	—	—
	3Si1B	0.24	2.8	0.5	0.5	0.09	−0.2	0.6	0.6	0.02	1.0	0.7	0.6	—	—	—	—
	2Si2B	0.19	−0.1	0.8	0.7	0.16	−0.6	0.6	0.6	0.03	0.9	0.7	0.5	—	—	—	—
	1Si3B	0.03	0.8	0.4	0.4	0.13	−0.1	0.5	0.6	0.19	−0.2	0.5	0.6	—	—	—	—
	4B	—	—	—	—	0.05	0.2	0.7	0.5	0.11	3.0	0.6	0.5	0.26	−0.6	0.6	0.6
Edén models																	
$B^{[3]}$	3Si	—	—	—	—	—	—	—	—	—	—	—	—	—	—	—	—
	2Si1B	0.05	15.3	2.6	0.3	0.07	14.7	2.6	0.2	0.03	13.9	2.6	0.2	—	—	—	—
	1Si2B	0.08	17.6	2.7	0.3	0.19	16.2	2.7	0.2	0.17	16.5	2.7	0.3	—	—	—	—
	3B	—	—	—	—	0.09	18.7	2.8	0.2	0.35	17.4	2.7	0.2	0.60	17.5	2.7	0.2
	2Si1NBO	0.24	16.7	2.4	0.7	—	—	—	—	—	—	—	—	—	—	—	—
$B^{[4]}$	4Si	0.09	−1.7	0.3	0.7	—	—	—	—	—	—	—	—	—	—	—	—
	3Si1B	0.19	−1.3	0.5	0.7	0.12	−1.0	0.4	0.6	—	—	—	—	—	—	—	—
	2Si2B	0.12	−0.1	0.6	0.7	0.14	−0.1	0.5	0.6	0.09	−0.4	0.3	0.6	—	—	—	—
	1Si3B	0.05	−0.1	0.7	0.7	0.11	−6.2	0.5	0.6	0.17	0.01	0.5	0.6	—	—	—	—
	4B	—	—	—	—	0.03	0.9	0.6	0.7	0.12	0.23	0.6	0.7	0.30	0.2	0.5	0.6

decreases with the Si-O-T angle thus a not negligible amount of the shift to negative values in the rigid ionic models is due to the larger angles concerning the ones found in structures generated with the shell model.

Indeed, Figure 2 shows that the ^{29}Si MAS NMR spectra generated using the Edén models are located to less negative δ_{iso} values and narrower concerning those computed with the rigid ionic models.

Another possible cause of the disagreement between simulated and experimental spectra could be the wrong population of different intermixing configurations possible among Si and B atoms in the second coordination sphere of silicon that can be indicated $Q^{n,m\mathrm{Si}p\mathrm{B}}$ (where $m + p = n$). However, the distributions of the T-O-T bridges (T = Si, B) generated by using the three potentials and which are reported in Table S7 of the ESI are similar.

Table 7 reports the isotropic chemical shifts of ^{29}Si as a function of the number of Si and B atoms in the second coordination sphere of Q^3 and Q^4 species in the investigated glasses. In general, the δ_{iso} of silicon seems to increase (it

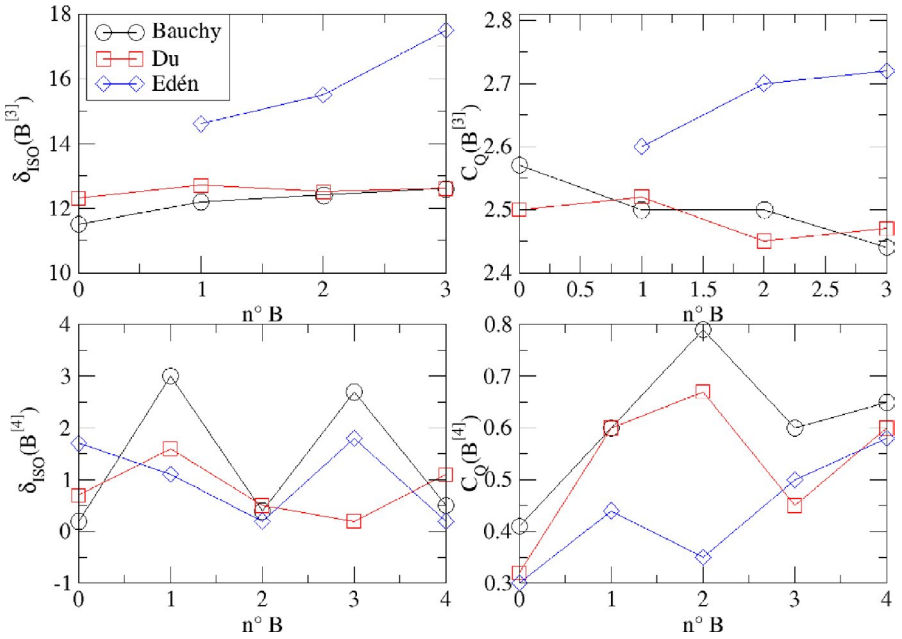

FIGURE 4 Average Isotropic chemical shifts (δ_{iso}) and quadrupolar coupling constants (C_Q) of $B^{[3]}$ and $B^{[4]}$ species in the investigated models as a function of the number of boron atoms in the second coordination sphere. The uncertainties on δ_{iso} and C_Q are of ±1.5 ppm and ±0.1 MHz, respectively

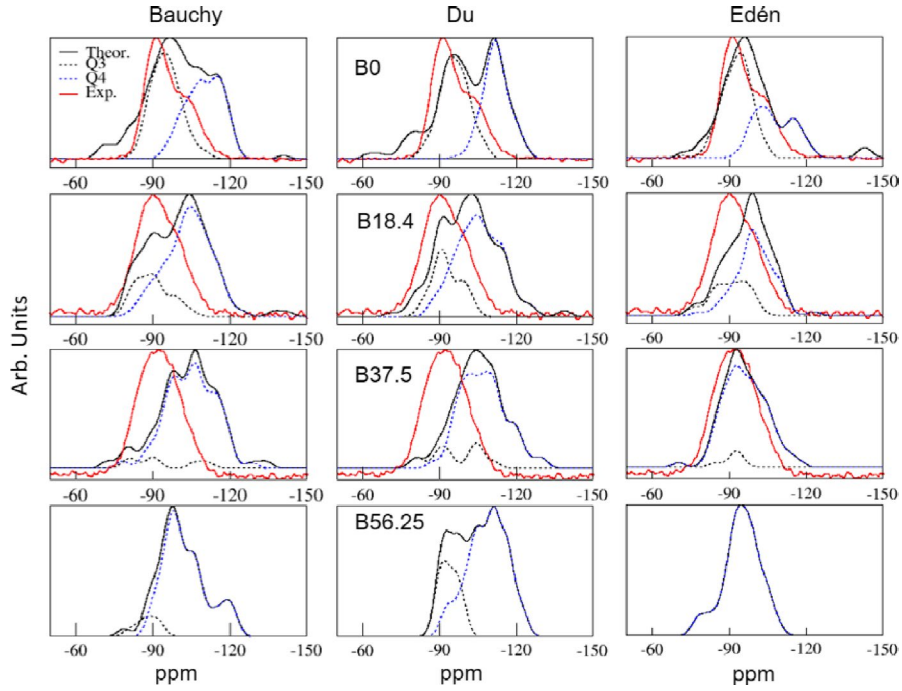

FIGURE 5 ^{29}Si MAS NMR of the investigated borosilicate glasses computed using structural models generated by using Bauchy (left), Du (middle), and Edén (right) potentials. The experimental spectra are reported in red. The magnetic field is 4.7 T. Spectra have been broadened using Gaussian functions with HWHM = 100 Hz. HWHM, half-width at half-maximum

becomes less negative) with the number of B atoms in the second coordination sphere. For example, it shifts from ~−92 ppm to ~−89.7 ppm for Q^3 species surrounded by 3Si and 3B respectively and from ~−107 ppm to ~−98.0 ppm for Q^4 species surrounded by 4Si and 4B in the B18.4 glass generated with the Bauchy potential. Similar trends are observed for the Du and Edén models.

It is interesting to note that this trend is clearer for Edén models. For example, the isotropic chemical shifts computed for the Q^4 species decrease from −106.2 ppm for $Q^{4,4Si}$ species to −101 ppm for $Q^{4,3Si1B}$ species to −99.7 ppm for $Q^{4,2Si2B}$ species to −97.0 ppm for $Q^{4,1Si,3B}$ in the B18.4 glass models and to −93.4 ppm for $Q^{4,4B}$ species in the B56.25 glass models.

Figure 6 shows that a linear relation exists between the average isotropic chemical shifts of Q^4 and Q^3 species computed considering all the glass models generated with Edén models and the number of boron atoms. The isotropic chemical shift of Q^4 and Q^3 species increases of ~3.35 and 1.5 ppm per boron atom, respectively.

These trends are in agreement with the observation that the average Si-O-Si angles are larger than Si-O-B ones. Moreover, the values computed on Edén's models are

TABLE 6 Q^n silicon species distributions of the simulated glasses using the Bauchy, Du, and Edén potentials before (in parenthesis) and after DFT geometry optimizations

		Q^1	Q^2	Q^3	Q^4	P^5
B0	Bauchy	0.67 (0.67)	10.0 (10.0)	43.3 (44.7)	44.7 (44.7)	1.3 (0.0)
	Du	2.0 (2.0)	7.3 (7.3)	46.0 (46.0)	44.7 (44.7)	0.0 (0.0)
	Edén	0.0 (0.0)	4.0 (4.7)	56.0 (57.3)	37.3 (38.0)	2.7 (0.0)
	Ref.[9]	—	—	67.1	32.9	—
B18.4	Bauchy	0.0 (0.0)	2.7 (2.7)	22.3 (19.6)	74.1 (77.7)	0.9 (0.0)
	Du	0.0 (0.0)	4.5 (4.5)	26.8 (22.3)	68.8 (73.2)	0.0 (0.0)
	Edén	0.0 (0.0)	0.0 (0.0)	29.5 (29.5)	70.5 (70.5)	0.0 (0.0)
	Ref.[9]	—	—	28.2	71.8	—
B37.5	Bauchy	0.0 (0.0)	0.0 (0.0)	13.2 (7.9)	85.5 (92.1)	1.3 (0.0)
	Du	0.0 (0.0)	0.0 (0.0)	17.1 (13.2)	82.9 (86.9)	0.0 (0.0)
	Edén	0.0 (0.0)	0.0 (0.0)	6.6 (6.6)	93.4 (93.4)	0.0
	Ref.[9]	—	—	8.2	91.8	—
B56.25	Bauchy	0.0 (0.0)	0.0 (0.0)	10.0 (2.5)	90.0 (97.5)	0.0 (0.0)
	Du	0.0 (0.0)	0.0 (0.0)	25.0 (20.0)	75.0 (80.0)	0.0
	Edén	0.0 (0.0)	0.0 (0.0)	0.0 (0.0)	100.0 (100)	0.0
	Ref.[9]	—	—	1.4	98.6	—

Abbreviation: DFT, density functional theory.

5-10 ppm smaller than that computed on the same glass using the Bauchy and Du potentials because of the smaller Si-O-T angles.

Bunker et al[52] and van Wuller et al[53] showed that the ^{29}Si isotropic chemical shift changes marginally when a Si-O-Si bond is replaced by Si-O-B$^{[3]}$ and more when it is replaced by a Si-O-B$^{[4]}$ bond, but the precise changes are not known. The knowledge of such changes could help to guide future deconvolutions of ^{29}Si NMR spectra and thus we have analyzed such changes by computing the $Q^{4,m\mathrm{Si}p\mathrm{B3kB4}}$ (where $m + p + k = 4$) species for the B18.4, B37.5, and B56.25 models generated with the three potentials. These data are reported in Tables S8-S10 of the ESI. We discuss here only the results obtained for the most populated Q^4 species with Edén models.

Table S10 shows that the δ_{iso} increases of about 4 ppm when a Si-O-Si bond of a $Q^{4,4\mathrm{Si}}$ is replaced by a Si-O-B$^{[3]}$ bond and of about 6 ppm when it is replaced by a Si-O-B$^{[4]}$ bond. Unfortunately, the populations of the other Q^n species do not allow us have clear and statistically robust trends but it seem that in general the substitution of a Si-O-B$^{[4]}$ or Si-O-B$^{[3]}$ bonds for Si-O-Si has a similar impact. Indeed, as observed above the Si-O-B$^{[4]}$ and Si-O-B$^{[3]}$ angles have similar values. Table 4 shows that the Si-O-B$^{[4]}$ angle is major or equal to Si-O-B$^{[3]}$ one for B18.4 and B56.25 glasses but minor for B37.5 glass.

3.3 | Sodium environment

The comparison between the simulated and experimental ^{23}Na MAS NMR spectra of the investigated glasses is reported in Figure 7. The agreement is good for all the models especially regarding peak positions. In general, the simulated spectra are more structured because of the reduced number of ions in the systems. However, it seems that the environment around sodium is fairly well reproduced after DFT optimizations even though in some cases the simulated spectra are rather broad concerning the experimental ones denoting that sodium environment in the computational models is more disordered than the real structures.

Table 8 reports the average Na-O bond distances and the average coordination numbers before and after DFT optimizations. In general, the average Na-O distances increase with the substitution of silicon by boron. Bauchy and Du potentials provide longer distances of 2.51-2.57Å and 2.45-2.57 Å than Edén potentials which range at 2.45-2.47 Å. The coordination numbers also increase from around 5.2-5.4 to 7.2-7.6, from B0 to B75 glasses. Albeit a shortening to 2.36-2.45 Å and a slight reduction in the coordination number is observed after DFT optimizations the trends with silicon/boron substitution are preserved.

These trends are associated with the shift of the peak position of the ^{23}Na MAS NMR spectra to more negative chemical shifts from B0 to B75 glasses as expected since sodium ions change their role from modifiers to charge compensator of BO_4 units. The NMR parameters reported as a function of the coordination number of sodium ions in Table S11-S13 seem to show no correlations between isotropic chemical shift and sodium coordination number, in agreement with the computational results obtained by Koller et al[54] and Gambuzzi et al[29] Correlations between ^{23}Na NMR parameters and Na coordination number was instead observed in several works on

TABLE 7 Population and isotropic chemical shift of Q^3 and Q^4 species in the borosilicate glasses generated with the Bauchy, Du, and Edén potentials. Only species with pop ≥ 0.02 have been tabulated

		$Q^{3,nSimB}$ (Si)				$Q^{4,nSimB}$(Si)				
		3Si	**2Si1B**	**1S12B**	**3B**	**4S1**	**3Si1B**	**2Si2B**	**1Si3B**	**4B**
Bauchy										
B0	pop	0.43	—	—	—	0.45	—	—	—	—
	δ_{iso}(ppm)	−95.5	—	—	—	−110.2	—		—	—
B18.4	pop	0.03	0.06	0.11	0.04	0.02	0.20	0.23	0.21	0.05
	δ_{iso}(ppm)	−92.3	−93.3	−88.18	−89.75	−107.2	−107.3	−105.4	−100.5	−97.7
B37.5	pop	0.01	—	0.08	0.03	—	0.01	0.16	0.37	0.32
	δ_{so}(ppm)	−89.0	—	−90.2	−109.2	—	−100.1	−106.4	−103.4	−107.1
B56.25	pop	—	—	—	0.10	—	—	0.03	0.30	0.58
	δ_{iso}(ppm)	—	—	—	−87.4	—	—	−99.5	−100.5	−103.8
Du										
B0	pop	0.46	—	—	—	0.45	—	—	—	—
	δ_{iso}(ppm)	−96.1	—	—	—	−112.4	—	—	—	—
B18.4	pop	0.07	0.09	0.08	0.03	0.04	0.19	0.21	0.20	0.03
	δ_{iso}(ppm)	−95.0	−93.8	−91.6	−93.9	−106.2	−107.6	−107.8	−103.5	−97.6
B37.5	pop	—	0.01	0.08	0.08	—	0.03	0.28	0.32	0.21
	δ_{so}(ppm)	—	−89.1	−94.8	−109.2	—	−100.1	−108.5	−107.4	−107.4
B56.25	pop	—	0.05	—	0.20	—	—	0.10	0.20	0.45
	δ_{iso}(ppm)	—	−93.7	—	−94.2	—	—	−105.0	−105.2	−111.4
Edén										
B0	pop	0.56	—	—	—	0.37	—	—	—	—
	δ_{iso}(ppm)	−93.03	—	—	—	107.8	—	—	—	—
B18.4	pop	0.12	0.12	0.04	—	0.07	0.27	0.23	0.13	—
	δ_{iso}(ppm)	−94.0	−88.6	−90.0	—	106.4	−101.0	−99.7	−97.9	—
B37.5	pop	—	0.03	0.03	—	—	0.09	0.41	0.28	0.16
	δ_{so}(ppm)	—	−92.6	−89.1	—	—	−98.9	−98.2	−96.4	−91.9
B56.25	pop	—	—	—	—	—	—	0.15	0.40	0.45
	δ_{iso}(ppm)	—	—	—	—	—	—	−99.0	−95.6	−93.4

crystalline compounds[55] where it was found that both δ_{iso} and C_Q generally decrease when CN increases. However, if the average δ_{iso} and C_Q of ^{23}Na of the different glasses is plotted against the average coordination number as in Figure 8 a correlation is observed for the isotropic chemical shift.

Figure 9 shows that in agreement with other DFT investigations,[29] a dependence of ^{23}Na δ_{iso} on average Na-O distance denoted as $\langle Na-O \rangle$ is observed when the coordination number is implicitly taken into account. No correlation is observed for η_Q.

4 | CONCLUSIONS

In this paper, we have used three recently developed interatomic potentials for boron based on the rigid ionic model (Bauchy and Du) and the shell model (Edén) in reproducing the structure of sodium borosilicate glasses. The evaluation of the performance of the three potential models has been carried out by comparing the MAS NMR spectra of ^{11}B, ^{23}Na, and ^{29}Si species computed at the DFT-GIPAW level on MD-derived models with up to 400 atoms. The effect of the DFT relaxation on the short-range structure has also been investigated to understand how the bond distances and angles obtained with the three potentials differ from the DFT values.

The main findings of this investigation are:

1. The rigid ionic parameterization proposed by Bauchy and Du well reproduce the N_3/N_4 partitioning in the whole compositional space investigated whereas the Edén potentials underestimate the N_4 fraction of the B18.4 glass which has a $[B_2O_3]/[SiO_2] \leq 0.33$.

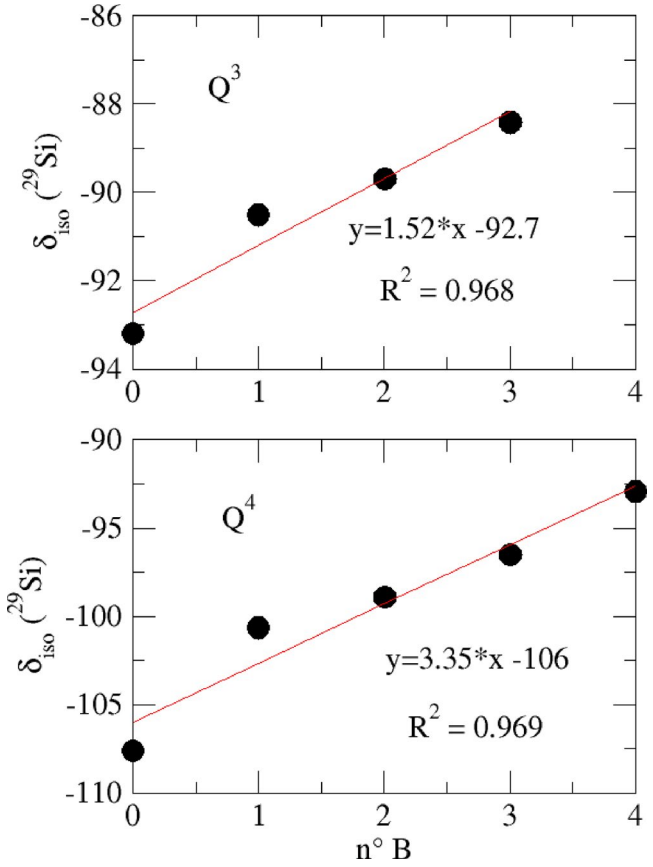

FIGURE 6 Correlation between the average isotropic chemical shift of Q^4 and Q^3 Si species considering all the glass models produced with Edén potentials

2. Among the three interatomic models, the one proposed by Edén slightly underestimates the $B^{[3]}$-O and the $B^{[4]}$-O bond distances whereas the Bauchy and Du potentials slightly overestimate them concerning the DFT values. Du potentials reproduce better the difference between the $B^{[3]}$-O and $B^{[4]}$-O bond length of 0.10-0.11 Å, also observed at the DFT level. This is probably the consequence of the dependency of the A parameter in the Buckingham function on the glass composition. However, it must be emphasized that all the potentials reproduce well these distances.
3. Edén potentials reproduce much better the silicon Q^n distributions, the intertetrahedra Si-O-T, B-O-T angles than the other two potentials, possibly due to the introduction of ion polarization effect in the potential. This is evidenced by the better agreement found with DFT data and the better reproduction of the ^{29}Si and ^{11}B MAS NMR spectral shapes of the glasses.
4. Bauchy and Du potentials overestimate the Na-O distances by around 0.1Å and coordination numbers by 0.1-0.8 concerning DFT values. However, after DFT relaxation the sodium environment is similar for all the MD-derived models. The fair reproduction of the ^{23}Na MAS NMR spectra indicates that sodium environment is well reproduced after DFT relaxation. In all the models, the structural role of sodium changes from network modifier to charge compensator with the substitution of B_2O_3 for SiO_2 in the glass.

Finally, we have also studied the correlation between NMR parameters and cation environments finding that:

1. The isotropic chemical shift of boron decreases with the B-O-T angle and with the amount of silicon in the second coordination sphere of boron. We have also observed that the substitution of $B^{[3]}/B^{[4]}$-O-$B^{[3]}$ bonds by $B^{[3]/[4]}$-O-$B^{[4]}$ bonds leads to an increase of the isotropic chemical shift.

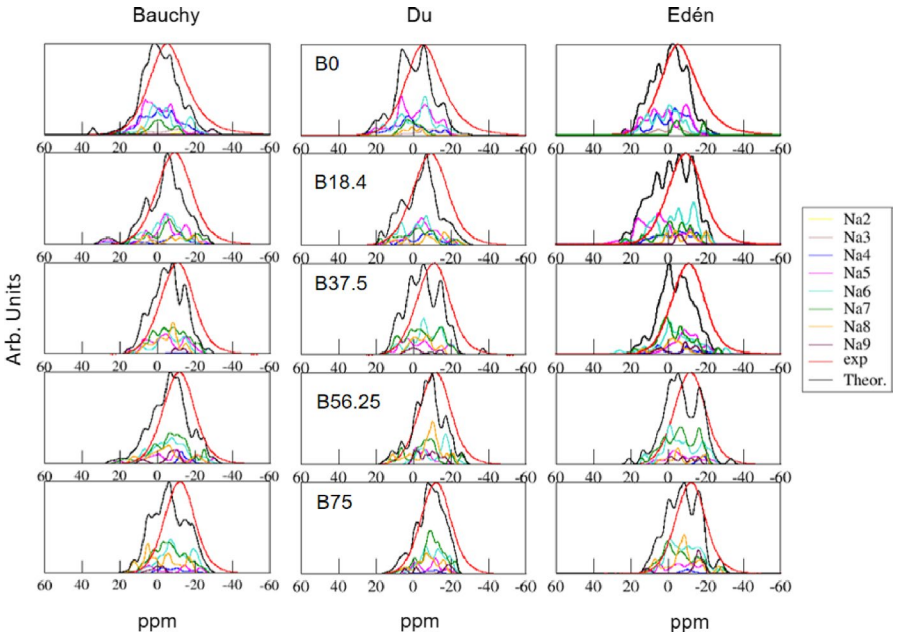

FIGURE 7 ^{23}Na MAS NMR of the investigated borosilicate glasses computed using structural models generated by using Bauchy (left), Du (middle), and Edén potentials. The experimental spectra are reported in red. The magnetic field used is 16.4 T. Spectra have been broadened using Gaussian functions with HWHM = 100 Hz. HWHM, half-width at half-maximum

TABLE 8 Average sodium coordination number (cutoff = 3.2 Å) of the simulated glasses using the Bauchy, Du, and Edén potentials computed after MM (in parenthesis) and after DFT geometry optimizations

	B0	B18.4	B37.5	B56.25	B75
Bauchy	5.1 (5.2)	5.9 (6.1)	6.6 (6.9)	6.7 (7.2)	6.8 (7.6)
Du	5.4 (5.4)	6.0 (6.3)	6.7 (7.1)	6.9 (7.5)	6.7 (7.5)
Edén	5.2 (5.2)	6.0 (6.1)	6.4 (6.7)	6.6 (7.0)	6.8 (7.2)

Abbreviation: DFT, density functional theory.

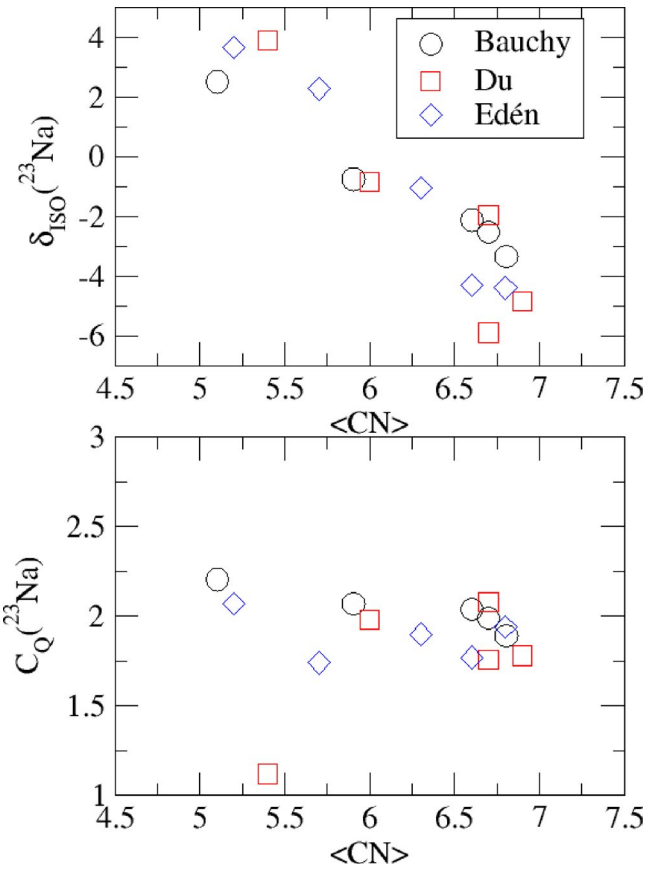

FIGURE 8 Correlation between (top) the average isotropic chemical shift and (bottom) average quadrupolar coupling constants of Na and the average coordination number computed for the investigated glasses. The uncertainties on δ_{iso} and C_Q are of ±2.0 ppm and ±0.5 MHz, respectively

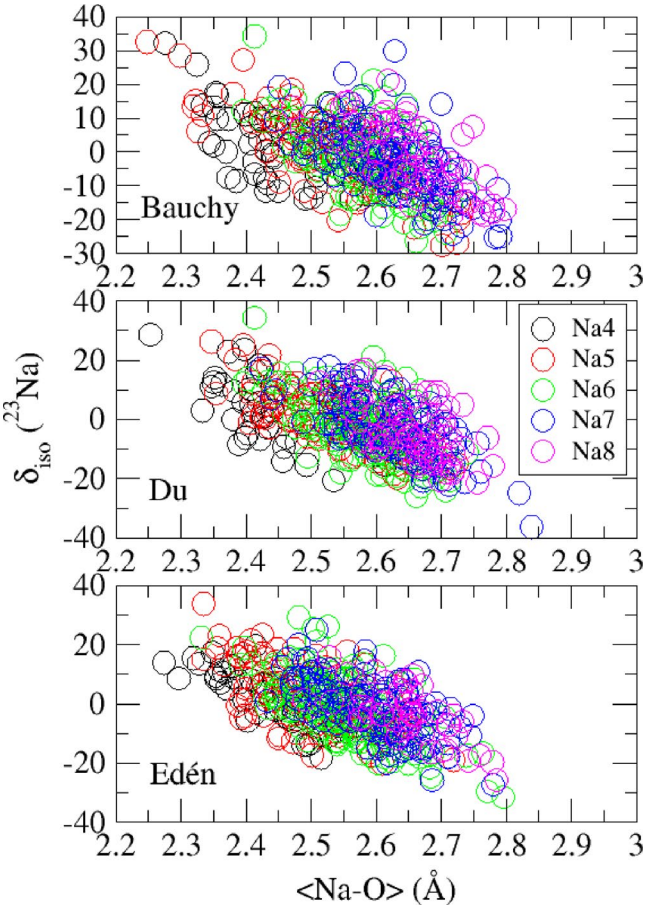

FIGURE 9 Correlations between δ_{iso} of ^{23}Na with the average Na-O distance for the Bauchy, Du, and Edén models

2. The isotropic chemical shift of silicon decreases with the Si-O-T angle and with the amount of boron in the second coordination sphere of silicon. An in-depth analysis of the second coordination sphere of silicon has shown that in general the substitution of a Si-O-B$^{[4]}$ or Si-O-B$^{[3]}$ bonds for Si-O-Si has a similar impact on the isotropic chemical shift. However, we have also observed that δ_{iso} increases of about 4 ppm when a Si-O-Si bond of a $Q^{4,4Si}$ is replaced by a Si-O-B$^{[3]}$ bond and of about 6 ppm when it is replaced by a Si-O-B$^{[4]}$ bond.
3. Regarding sodium, we have observed that the average δ_{iso} of ^{23}Na of the different glasses decreases with the average coordination number whereas no correlation is observed for the quadrupolar coupling constant and asymmetry parameter. Moreover, a dependence of ^{23}Na δ_{iso} on average Na-O distance is observed when the coordination number is implicitly taken into account.

As final considerations, it is worth to underline that the DFT optimization performed before the calculation of NMR parameters might improve the results obtained using the rigid ionic models more than the ones obtained with

the shell model since the DFT relaxation leads to a significant reduction of the T-O-T angle in the former case. While the sodium environments were significantly modified for all the force fields used after DFT relaxation. Moreover, as already noted by Wang et al[17] the fact that all the interatomic potentials reproduce well the N_4 fraction is due to a "cancellation of errors" since it is well known that boron coordination depends on the thermal history of the glass.[48,56] Our MD results would be better compared with hyperquenched glasses that exhibit lower fractions of four-fold coordinated B atoms.

However, it must also be pointed out that the high computational cost makes classical molecular dynamics intrinsically limited to the use of relatively high cooling rates. Additionally, as discussed by Corrales and Du,[57] MD simulations of glasses use relatively small system sizes (typically a few thousands to tens of thousands as compared to real glass with Avogadro's number of atoms) with periodic boundary conditions. With such, the energy exchange between particles is faster than the real system thus the higher cooling rate employed might be fine for generating glass structures and was reflected in the comparable to experimental glass structures for silicate glasses.[57] In this respect, classical MD simulation could be considered as an effective tool to generate reliable structural models of glasses and is indeed the most widely used atomistic simulation method for glass materials.

ACKNOWLEDGMENTS

This material is based on work supported by the U.S. National Science Foundation under Grant Nos. 1507131 and 1508001.

ORCID

Lu Deng https://orcid.org/0000-0002-5912-3908
Ashutosh Goel https://orcid.org/0000-0003-0139-9503
Jincheng Du https://orcid.org/0000-0003-4805-7498
Alfonso Pedone https://orcid.org/0000-0003-3772-7222

REFERENCES

1. Pye LD, Fréchette VD, Borate K. Borate glasses: structure, properties, applications. Materials science research. US: Springer; 1978. Available from //www.springer.com/us/book/9781468433593
2. Fu Q, Rahaman MN, Fu H, Liu X. Silicate, borosilicate, and borate bioactive glass scaffolds with controllable degradation rate for bone tissue engineering applications. I. preparation and in vitro degradation. J Biomed Mater Res Part A. 2010;95A(1):164–71.
3. Lusvardi G, Malavasi G, Tarsitano F, Menabue L, Menziani MC, Pedone A. Quantitative structure-property relationships of potentially bioactive fluoro phospho-silicate glasses. J Phys Chem B. 2009;113(30):10331–8.
4. Pedone A, Menziani MC. Computational modeling of silicate glasses: a quantitative structure-property relationship perspective. In: Massobrio C, Du J, Bernasconi M, Salmon PS, Curatori, editors. Molecular dynamics simulations of disordered materials: from network glasses to phase-change memory alloys. Springer series in materials science. Cham, Switzerland: Springer International Publishing, 2015; p. 113–35. https://doi.org/10.1007/978-3-319-15675-0_5
5. Pedone A. Properties calculations of silica-based glasses by atomistic simulations techniques: a review. J Phys Chem C. 2009;113(49):20773–84.
6. Tilocca A, Cormack AN, deLeeuw NH. The structure of bioactive silicate glasses: new insight from molecular dynamics simulations. Chem Mater. 2007;19(1):95–103.
7. Xiang Y, Du J. Effect of strontium substitution on the structure of 45S5 bioglasses. Chem Mater. 2011;23(11):2703–17.
8. Chen X, Chen X, Pedone A, Apperley D, Hill RG, Karpukhina N. New insight into mixing fluoride and chloride in bioactive silicate glasses. Sci Rep. 2018;8:1316.
9. Stone-Weiss N, Pierce EM, Youngman RE, Gulbiten O, Smith NJ, Du J, et al. Understanding the structural drivers governing glass–water interactions in borosilicate based model bioactive glasses. Acta Biomater. 2018;65:436–49.
10. Konijnendijk WL, Stevels JM. The structure of borate glasses studied by Raman scattering. J Non-Cryst Solids. 1975;18(3):307–31.
11. Yun YH, Bray PJ. Nuclear magnetic resonance studies of the glasses in the system $Na_2O{\cdot}B_2O_3{\cdot}SiO_2$. J Non-Cryst Solids. 1978;27(3):363–80.
12. Hubert M, Faber AJ. On the structural role of boron in borosilicate glasses. Phys Chem Glas-Eur J Glass Sci Technol Part B. 2014;55(3):136–58.
13. Delaye J-M, Ghaleb D. Molecular dynamics simulation of $SiO_2{\cdot}B_2O_3{\cdot}Na_2O{\cdot}ZrO_2$ glass. J Non-Cryst Solids. 1996;195(3):239–48.
14. Gou F, Greaves GN, Smith W, Winter R. Molecular dynamics simulation of sodium borosilicate glasses. J Non-Cryst Solids. 2001;1(293–295):539–46.
15. Kieu L-H, Delaye J-M, Cormier L, Stolz C. Development of empirical potentials for sodium borosilicate glass systems. J Non-Cryst Solids. 2011;357(18):3313–21.
16. Inoue H, Masuno A, Watanabe Y. Modeling of the structure of sodium borosilicate glasses using pair potentials. J Phys Chem B. 2012;116(40):12325–31.
17. Wang M, Krishnan N, Wang B, Smedskjaer MM, Mauro JC, Bauchy M. A new transferable interatomic potential for molecular dynamics simulations of borosilicate glasses. J Non-Cryst Solids. 2018;498:294–304.
18. Deng L, Du J. Development of boron oxide potentials for computer simulations of multicomponent oxide glasses. J Am Ceram Soc. 2018;102:1–24.
19. Stevensson B, Yu Y, Edén M. Structure–composition trends in multicomponent borosilicate-based glasses deduced from molecular dynamics simulations with improved B-O and P–O force fields. Phys Chem Chem Phys. 2018;20(12):8192–209.
20. Pacaud F, Delaye J-M, Charpentier T, Cormier L, Salanne M. Structural study of $Na_2O–B_2O_3–SiO_2$ glasses from

molecular simulations using a polarizable force field. J Chem Phys. 2017;147(16):161711.
21. Aguado A, Bernasconi L, Madden PA. Interionic potentials from ab initio molecular dynamics: the alkaline earth oxides CaO, SrO, and BaO. J Chem Phys. 2003;118(13):5704–17.
22. Tilocca A. Short- and medium-range structure of multicomponent bioactive glasses and melts: an assessment of the performances of shell-model and rigid-ion potentials. J Chem Phys. 2008;129(8):084504.
23. Yu Y, Stevensson B, Edén M. Medium-range structural organization of phosphorus-bearing borosilicate glasses revealed by advanced solid-state NMR experiments and MD simulations: consequences of B/Si substitutions. J Phys Chem B. 2017;121(41):9737–52.
24. Yu Y, Stevensson B, Edén M. Direct experimental evidence for abundant BO_4–BO_4 motifs in borosilicate glasses from double-quantum ^{11}B NMR spectroscopy. J Phys Chem Lett. 2018;9(21):6372–6.
25. Pickard CJ, Mauri F. All-electron magnetic response with pseudopotentials: NMR chemical shifts. Phys Rev B. 2001;63(24):245101.
26. Blöchl PE. Projector augmented-wave method. Phys Rev B. 1994;50(24):17953–79.
27. Charpentier T. The PAW/GIPAW approach for computing NMR parameters: a new dimension added to NMR study of solids. Solid State Nucl Magn Reson. 2011;40(1):1–20.
28. Gambuzzi E, Pedone A, Menziani MC, Angeli F, Caurant D, Charpentier T. Probing silicon and aluminium chemical environments in silicate and aluminosilicate glasses by solid state NMR spectroscopy and accurate first-principles calculations. Geochim Cosmochim Acta. 2014;15(125):170–85.
29. Gambuzzi E, Charpentier T, Menziani MC, Pedone A. Computational interpretation of ^{23}Na MQMAS NMR spectra: a comprehensive investigation of the Na environment in silicate glasses. Chem Phys Lett. 2014;18(612):56–61.
30. Charpentier T, Menziani MC, Pedone A. Computational simulations of solid state NMR spectra: a new era in structure determination of oxide glasses. Rsc Adv. 2013;3(27):10550–78.
31. Pedone A, Charpentier T, Menziani MC. Multinuclear NMR of $CaSiO_3$ glass: simulation from first-principles. Phys Chem Chem Phys. 2010;12(23):6054–66.
32. Pedone A, Gambuzzi E, Malavasi G, Menziani MC. First-principles simulations of the ^{27}Al and ^{17}O solid-state NMR spectra of the $CaAl_2Si_3O_{10}$ glass. Theor Chem Acc. 2012;131(3):1147.
33. Pedone A, Gambuzzi E, Menziani MC. Unambiguous description of the oxygen environment in multicomponent aluminosilicate glasses from ^{17}O solid state NMR computational spectroscopy. J Phys Chem C. 2012;116(27):14599–609.
34. Segall MD, Lindan P, Probert MJ, Pickard CJ, Hasnip PJ, Clark SJ, et al. First-principles simulation: ideas, illustrations and the CASTEP code. J Phys-Condens Matter. 2002;14(11):2717–44.
35. Dell WJ, Bray PJ, Xiao SZ. ^{11}B NMR studies and structural modeling of Na_2O B_2O_3 SiO_2 glasses of high soda content. J Non-Cryst Solids. 1983;58(1):1–16.
36. Dick BG, Overhauser AW. Theory of the dielectric constants of alkali halide crystals. Phys Rev. 1958;112(1):90–103.
37. Smith W, Forester TR. DL_POLY_2.0: a general-purpose parallel molecular dynamics simulation package. J Mol Graph. 1996;14(3):136–41.
38. Malavasi G, Pedone A, Menziani MC. Study of the structural role of gallium and aluminum in 45S5 bioactive glasses by molecular dynamics simulations. J Phys Chem B. 2013;117(15):4142–50.
39. Allen MP, Allen MP, Tildesley DJ, Tildesley DJ. Computer simulation of liquids. Oxford: Clarendon Press, 1989; p. 412.
40. Perdew JP, Burke K, Ernzerhof M. Generalized gradient approximation made simple. Phys Rev Lett. 1996;77(18):3865–8.
41. Pedone A, Charpentier T, Malavasi G, Menziani MC. New insights into the atomic structure of 45S5 bioglass by means of solid-state NMR spectroscopy and accurate first-principles simulations. Chem Mater. 2010;22(19):5644–52.
42. Alderman O, Iuga D, Howes AP, Pike KJ, Holland D, Dupree R. Spectral assignments and NMR parameter-structure relationships in borates using high-resolution ^{11}B NMR and density functional theory. Phys Chem Chem Phys. 2013;15(21):8208–21.
43. Pyykkö P. Year-2008 nuclear quadrupole moments. Mol Phys. 2008;106(16–18):1965–74.
44. Presti D, Pedone A, Licari D, Barone V. A modular implementation for the simulation of 1D and 2D solid-state NMR spectra of quadrupolar nuclei in the virtual multifrequency spectrometer-draw graphical interface. J Chem Theory Comput. 2017;13(5):2215–29.
45. Fukushima E, Roeder S. Experimental pulse NMR: a nuts and bolts approach. Oxford: Addison-Wesley, 1993; p. 558.
46. Kim J. Chemical shift and quadrupolar interactions in solids. J Korean Magn Reson Soc. 2006;10:1–37.
47. Angeli F, Villain O, Schuller S, Charpentier T, de Ligny D, Bressel L, et al. Effect of temperature and thermal history on borosilicate glass structure. Phys Rev B. 2012;85(5):054110.
48. Pedesseau L, Ispas S, Kob W. First-principles study of a sodium borosilicate glass-former. I. the liquid state. Phys Rev B. 2015;91(13):134201.
49. Swenson J, Börjesson L, Howells WS. Structure of borate glasses from neutron-diffraction experiments. Phys Rev B Condens Matter. 1995;52(13):9310–9.
50. Pedone A, Charpentier T, Menziani MC. The structure of fluoride-containing bioactive glasses: new insights from first-principles calculations and solid state NMR spectroscopy. J Mater Chem. 2012;22(25):12599–608.
51. Pedone A, Pavone M, Menziani MC, Barone V. Accurate first-principle prediction of ^{29}Si and ^{17}O NMR Parameters in SiO_2 polymorphs: the cases of zeolites sigma-2 and ferrierite. J Chem Theory Comput. 2008;4(12):2130–40.
52. Bunker BC, Tallant DR, Kirkpatrick RJ, Turner GL. Multinuclear nuclear magnetic resonance and Raman investigation of sodium borosilicate glass structures. Phys Chem Glas. 1990;31(1):30–41.
53. van Wüllen L, Müller-Warmuth W, Papageorgiou D, Pentinghaus HJ. Characterization and structural developments of gel-derived borosilicate glasses: a multinuclear MAS-NMR study. J Non-Cryst Solids. 1994;171(1):53–67.
54. Koller H, Engelhardt G, Kentgens A, Sauer J. ^{23}Na NMR spectroscopy of solids: interpretation of quadrupole interaction parameters and chemical shifts. J Physial Chem. 1994;98(6):1544–51.
55. Antonijevic S, Ashbrook SE, Walton RI, Wimperis S. A multiple-quantum ^{23}Na MAS NMR study of amorphous sodium gallium silicate zeolite precursors. J Mater Chem. 2002;12(5):1469–74.
56. Smedskjaer MM, Mauro JC, Youngman RE, Hogue CL, Potuzak M, Yue Y. Topological principles of borosilicate glass chemistry. J Phys Chem B. 2011;115(44):12930–46.

57. Corrales LR, Du J. Thermal kinetics of glass simulations. Phys Chem Glasses. 2005;46:420–4.

SUPPORTING INFORMATION

Additional supporting information may be found online in the Supporting Information section at the end of the article.

How to cite this article: Fortino M, Berselli A, Stone-Weiss N, et al. Assessment of interatomic parameters for the reproduction of borosilicate glass structures via DFT-GIPAW calculations. *J Am Ceram Soc*. 2019;00:1–19. https://doi.org/10.1111/jace.16655